Progress in Natural Science: Materials International 26 (2016) 440–448

HOSTED BY

Contents lists available at ScienceDirect

Progress in Natural Science: Materials International

journal homepage: www.elsevier.com/locate/pnsmi

Review

Structural effects on the magnetic hyperthermia properties of iron oxide nanoparticles

Eric C. Abenojar[a], Sameera Wickramasinghe[a], Jesbaniris Bas-Concepcion[a,b], Anna Cristina S. Samia[a,*]

[a] Department of Chemistry, Case Western Reserve University, Cleveland, OH 44106, USA
[b] Chemistry Department, University of Puerto Rico, Rio Piedras Campus, San Juan, PR 00931, USA

ARTICLE INFO

Keywords:
Iron oxide nanoparticles
Magnetic hyperthermia
Magneto-structural effects
Magnetic dipolar interactions
Magnetic imaging guided – hyperthermia

ABSTRACT

Magnetic iron oxide nanoparticles (IONPs) are heavily explored as diagnostic and therapeutic agents due to their low cost, tunable properties, and biocompatibility. In particular, upon excitation with an alternating current (AC) magnetic field, the NPs generate localized heat that can be exploited for therapeutic hyperthermia treatment of diseased cells or pathogenic microbes. In this review, we focus on how structural changes and inter-particle interactions affect the heating efficiency of iron oxide-based magnetic NPs. Moreover, we present an overview of the different approaches to evaluate the heating performance of IONPs and introduce a new theranostic modality based on magnetic imaging guided–hyperthermia.

1. Introduction

Iron oxide nanoparticles (IONPs) are widely investigated due to their tunable magnetic properties and potential as diagnostic (i.e. as magnetic resonance imaging contrast agents and magnetic particle imaging tracers) and therapeutic (e.g. drug and gene delivery, hyperthermia) agents [1–23]. Upon excitation with an AC field, these unique materials can transform electromagnetic energy to heat, and the heat generated can be utilized to destroy cancer cells or pathogenic microbes. In magnetic hyperthermia, the heating can occur by any of the three mechanisms: (1) eddy current heating due to the effects of induction from the application of an alternating pulsed magnetic field; (2) frictional heating induced by the interaction between the NPs and the surrounding medium, and (3) relaxation and hysteretic losses of the magnetic NPs [24].

The use of IONPs for magnetic hyperthermia treatment of cancers was first demonstrated by Gilchrist et al. in 1957 [25]. Following this seminal work, various groups have investigated the important operational parameters to effectively carry out the use of magnetic hyperthermia in cancer therapy [26–28]. In 2004, the first clinical magnetic hyperthermia treatment system was developed at Charité – Medical University of Berlin [29], and a few years later, *Magforce*® obtained European regulatory approval to treat patients with brain tumor using magnetic hyperthermia [30]. Over the years, the utility of magnetic hyperthermia has been extended to other applications including heat triggered drug delivery [31–34], biofilm inactivation [35,36], and fabrication of smart heat responsive materials [37].

While magnetic hyperthermia has been clinically approved for brain tumor treatment in Europe, it is still not widely utilized in the clinic. Particularly, magnetic hyperthermia has not been approved as a treatment approach in hospitals in the USA and other parts of the world. The lack of widespread adaptation of this treatment modality can be partly attributed to gaps in the development of optimized magnetic NP hyperthermia agents.

Shown in Fig. 1 is a schematic representation of the important parameters (i.e. optimization of the magneto-structural properties of magnetic NPs, magnetic dipolar interaction effects, reliability of the methods used in magnetic hyperthermia measurements) that need to be addressed in designing IONPs with optimized heating efficiency for various magnetic hyperthermia applications (e.g. magnetic imaging-guided hyperthermia, magnetic actuated drug delivery, thermal cancer therapy, biofilm eradication). To date, several excellent review articles have been published, which focused on the different synthetic routes that have been developed to prepare IONPs with different morphologies and surface chemistries [4,9–12,15,17,22,38–40], while some articles have detailed the different heat release mechanisms in magnetic hyperthermia [41,42]. In this review article, we will center the discussion on how the different structural motifs such as NP size, composition, morphology, and nano-assemblies (i.e. clustering and chaining) affect the magnetic hyperthermia properties and heating

Peer review under responsibility of Chinese Materials Research Society.
* Corresponding author.
E-mail address: anna.samia@case.edu (A.C.S. Samia).

http://dx.doi.org/10.1016/j.pnsc.2016.09.004
Received 31 July 2016; Accepted 16 August 2016
Available online 05 October 2016

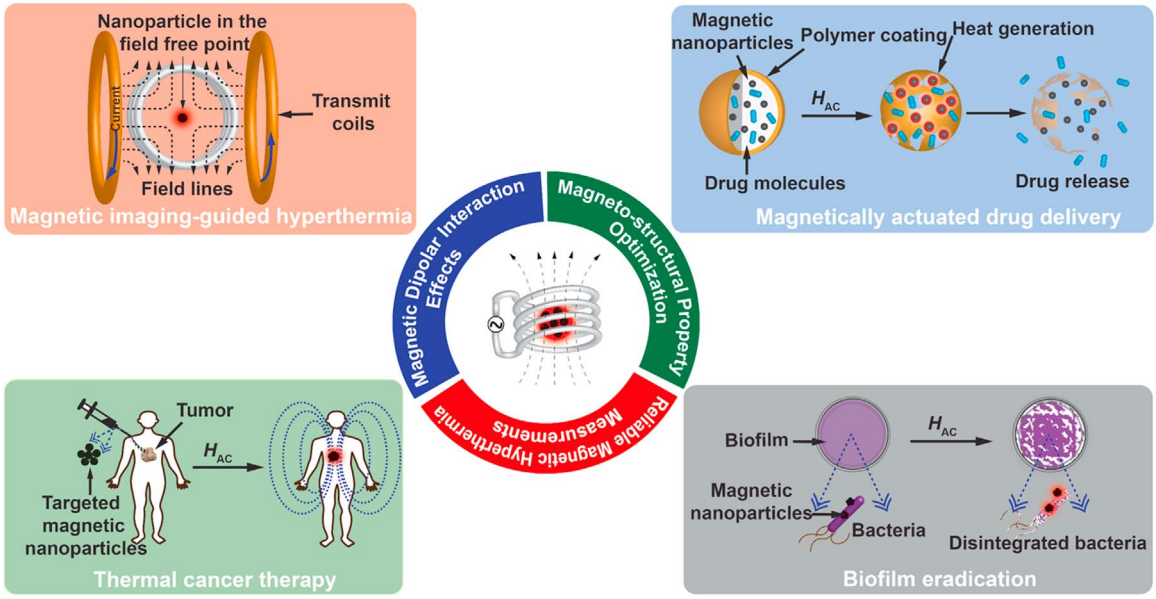

Fig. 1. Schematic diagram illustrating the important parameters affecting the efficiency of magnetic hyperthermia treatment and the different types of biomedical magnetic hyperthermia applications.

efficiency of iron oxide-based NPs.

2. Basic principles and measurements in magnetic hyperthermia

2.1. Magnetic behavior of single domain nanoparticles

The Stoner-Wohlfarth (SW) model describes the magnetic behavior of a single domain NP (Fig. 2a) [43]. The total energy (E) of such a system is defined by both the anisotropy energy (E_A) and the Zeeman energy (E_z):

$$E = E_A + E_z = KV\sin^2\theta - HVM_s\cos(\theta-\phi) \quad (1)$$

where, K is the uniaxial magnetic anisotropy, H is the applied field, V is the NP volume, M_s is the saturation magnetization, θ is the angle between the easy axis and the NP magnetization, and ϕ is the angle between the easy axis and the applied magnetic field. At $H = 0$, the energy barrier is equivalent to KV and for systems wherein the anisotropy energy barrier is comparable to the thermal activation energy ($KV \sim k_B T$), magnetic moment switching becomes feasible leading to superparamagnetic behavior.

Superparamagnetism involves the thermal activated switching of the magnetic moment of a NP. This occurs above the so-called blocking temperature (T_B), which is described by the equation,

$$T_B = \frac{KV}{k_B \ln(\tau_m/\tau_0)} \quad (2)$$

where, k_B is the Boltzmann constant, τ_m is the measurement time, and τ_0 is the attempt time, which is typically approximated as 10^{-9} s. For magnetite (Fe_3O_4) NPs, superparamagnetic behavior at room temperature typically occurs at particle sizes smaller than 25 nm in diameter [16].

2.2. Heating of magnetic nanoparticles in an AC field

Various models and experimental data have been employed to better understand the heating process in magnetic hyperthermia [41–47]. In 2002, Rosensweig developed the linear response theory (LRT) to explain the heating of colloidal magnetic fluids subjected to an alternating magnetic field [44]. In his formulation, it was assumed that the heat generation was only due to the rotational relaxation of non-interacting single domain NPs, and the magnetization of the NPs varies linearly with the applied magnetic field. From the LRT model, an expression for the power dissipation (P) was derived as follows [44]:

$$P = \mu_0 \pi \chi'' f H^2 \quad (3)$$

where, H and f are the amplitude and frequency of the AC magnetic field, respectively, μ_0 represents the permeability of free space, and χ'' is the out-of-phase component of the colloidal magnetic fluid AC susceptibility. In turn, χ'' can be expressed as:

$$\chi'' = \frac{\omega\tau}{1+(\omega\tau)^2}\chi_0 \quad (4)$$

where, $\omega = 2\pi f$, χ_0 is the actual susceptibility, and τ is the effective

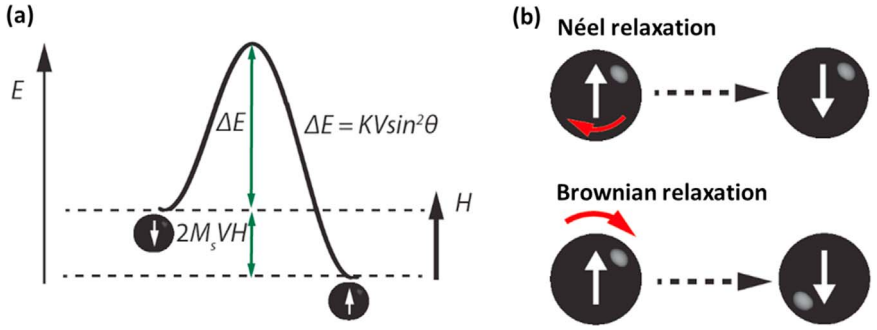

Fig. 2. (a) Representation of the energy barriers governing single domain particles. (b) Relaxation processes that influence the heating properties of magnetic nanoparticles.

relaxation time. The effective relaxation time is dependent on the collective contributions of both Néel and Brownian relaxation processes (Fig. 2b). Néel relaxation involves the internal rotation of the magnetic moment and has a characteristic time, τ_N, which is expressed as:

$$\tau_N = \left(\frac{\sqrt{\pi}}{2}\right)\tau_0 \frac{\exp\left(\frac{KV}{k_BT}\right)}{\sqrt{\frac{KV}{k_BT}}} \quad (5)$$

On the other hand, Brownian relaxation pertains to the physical rotation of the magnetic NP itself and the characteristic relaxation time, τ_B, is represented in the following equation:

$$\tau_B = \frac{3\eta V_H}{k_BT} \quad (6)$$

where, η is the dynamic viscosity and V_H is the hydrodynamic volume. The effective relaxation time can then be expressed as:

$$\frac{1}{\tau} = \frac{1}{\tau_B} + \frac{1}{\tau_N} \quad (7)$$

Substituting Eq. (4) into Eq. (3) results in an expanded form of the power dissipation expression:

$$P = \mu_0 \pi \chi_0 f H^2 \left(\frac{2\pi f\tau}{1+[2\pi f\tau]^2}\right) \quad (8)$$

which showcases the dependence of the heat generation process with the frequency and amplitude of the applied AC field, and the magnetic NP relaxation processes.

The heating efficiency is represented by the specific loss power (SLP) also referred to as the specific absorption rate (SAR), which is defined as the ratio of the heat power dissipated and the mass of the magnetic NPs, m_{MNP}:

$$SLP = \frac{P}{m_{MNP}} \quad (9)$$

One limitation of the SLP representation is its dependence with H^2, which makes direct comparison of reported literature values difficult owing to variations in the applied AC field conditions. To address this issue, the intrinsic loss power (ILP) can be calculated whereby the SLP is normalized to the AC field strength and frequency [48]:

$$ILP = \frac{SLP}{fH^2} \quad (10)$$

The ILP representation, however, is only applicable at low field strengths and low frequency AC excitations.

2.3. Magnetic hyperthermia measurement

2.3.1. Calorimetric method

The calorimetric approach is the most commonly adapted method in evaluating the magnetic hyperthermia properties of magnetic NPs. In this method, the temperature increase in the sample is recorded over a period of time as the magnetic NPs are exposed to an AC field of a particular amplitude and frequency (Fig. 3a). A fiber optic temperature probe is typically used in conjunction with a magnetic induction heating system consisting of a water cooled coil that is connected to a high power *rf* generator. Samples are placed in a thermally insulated container to avoid heat loss to the environment during measurement, and the SLP is calculated from the temperature derivative over time at instant $t = 0$as,

$$SLP = \frac{CV_s}{m_{MNP}} \bullet \left.\frac{dT}{dt}\right|_{t=0} \quad (11)$$

where,C is the volumetric specific heat capacity of the sample solution, V_s is the sample volume, m is the mass of the magnetic material, and dT/dt is the initial slope of the change in temperature versus time curve.

Evaluation of the heating efficiency using the calorimetric method is ideal when measurements are performed under adiabatic conditions where there is no heat exchange between the sample and the surroundings [50]. To eliminate conduction, convection, and thermal radiation heat losses, high vacuum conditions and adiabatic shields are used during measurements [51]. However, such systems are costly and difficult to set-up and operate; hence, adiabatic systems are rarely used in calorimetric magnetic hyperthermia measurements [50-52].

On the other hand, the heating efficiency evaluated using non-adiabatic systems shows an average decrease of about 21% in the measured SLP value [51]. However, non-adiabatic systems are commonly adopted because of the quick measurement time and ease of operation. By taking into account all the thermal losses from a non-adiabatic set-up it can also be a reliable approach to measure the heating efficiency of magnetic NPs [53]. In a non-adiabatic system, the heating curve starts to drop as higher temperatures are reached due to thermal losses (Fig. 3a). Wildeboer et al. proposed an alternative method to better evaluate the SLP by adding a thermal loss parameter, L, which can be estimated by determining the slope for multiple temperatures along the heating curves [53].

$$SLP_{correctedslope} = \frac{(CV_s\frac{dT}{dt} + L\Delta T)}{m_{MNP}} \quad (12)$$

where, ΔT is the average temperature difference between the sample and the baseline.

2.3.2. Magnetometric method

A second approach that can be employed to evaluate the heating efficiency in magnetic hyperthermia is based on the measurement of the dynamic magnetization $M(t)$ of the sample. In the magnetometric method, the SLP can be calculated by integrating (performed over one period $2\pi/f$) the dynamic magnetization with respect to the applied field strength [49,54]:

$$SLP = \frac{f}{c}\oint M(t)\, dH \quad (13)$$

where, f is the frequency and$c$ is the weight concentration of the NP. In this approach the SLP is proportional to the area of the AC hysteresis loop (A_{hys}) as illustrated in Fig. 3b.

3. Structural effects on magnetic hyperthermia properties of IONPs

During magnetic hyperthermia measurements, the power dissipated is dependent on the intrinsic magnetic properties of the IONPs, which influences its relaxation (Néel and Brownian) and hysteretic losses (AC field effects and magnetic dipolar interaction effects). Based on the LRT model, the heating efficiency is proportional to the saturation magnetization of the magnetic NP but peaks at a certain NP size (volume) and magnetic anisotropy [8,44]. The optimum NP size and crystalline anisotropy also depend on the strength and frequency of the applied AC field. Magnetic dipolar interactions that promote the formation of nano-assemblies organized as nanoclusters or nanochains, can also modify the relaxation behavior of the magnetic NPs. In the succeeding sections, the structural effects (size, composition, shape, exchange-coupling, formation of nano-assemblies) on the heating efficiency of IONPs will be discussed to provide a better understanding on how each materials parameter can be optimized for magnetic hyperthermia applications.

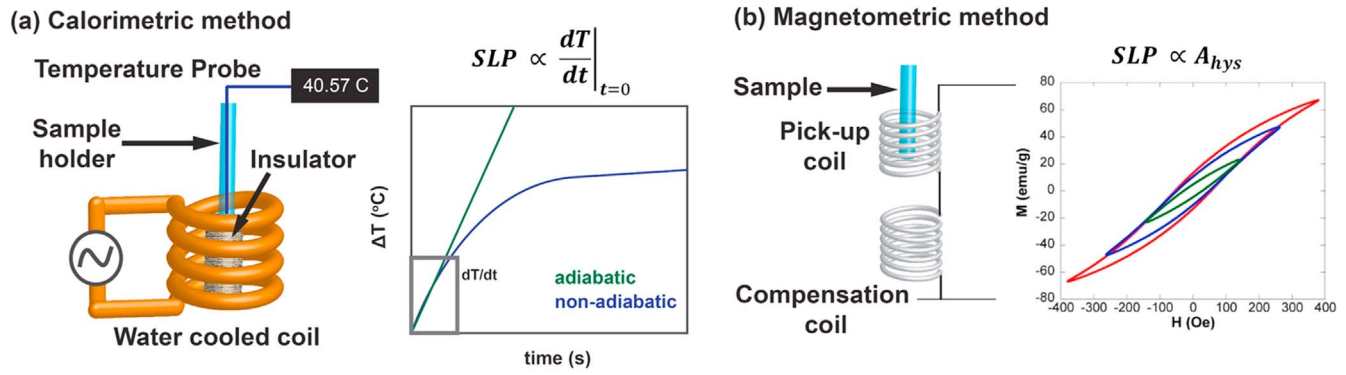

Fig. 3. Schematic diagram of the different approaches used to evaluate the heating efficiency of magnetic nanoparticles: (a) calorimetric method, wherein the changes in the temperature of the sample is recorded as it is exposed to an AC field excitation (the SLP is calculated from the initial slope of the change in temperature vs. time curve); and (b) magnetometric method, which involves the measurement of the AC susceptibility of the sample wherein the SLP is proportional to the area of the hysteresis curve. The hysteresis plot was adapted with permission from reference [49] copyright (2016) American Chemical Society.

3.1. Size dependence of the magnetic hyperthermia properties of superparamagnetic nanoparticles

Changing the size of IONPs dramatically alters its response to an applied AC field. Superparamagnetic NPs are governed by size dependent Néel and Brownian relaxation losses, which in turn directly affect the heat power dissipation process. The magnetization of IONPs decreases with decreasing particle size [55]. Owing to their small size, magnetic IONPs exhibit low saturation magnetization due to surface and internal spin canting effects [56,57]. Spin-spin exchange coupling gives rise to magnetically disordered spin glass-like layers on the surface of magnetic NPs, which is not readily observed in bulk magnetic materials [56,57]. In addition, the presence of a magnetically frustrated layer on the NP surface, due to incomplete coordination of the metal ions, also lowers the magnetization of magnetic NPs [58].

Because the SLP value is dependent on the magnetization and relaxation time of the NP, for a given magnetic material there is an optimum size that will result in enhanced hyperthermia effects [44]. For superparamagnetic IONPs, Vreeland et al. observed that for an AC excitation field of $H = 36.5$ kA/m and $f = 341$ kHz, the optimum size showing maximum SLP was around 22 nm, which matches the theoretical prediction of the LRT [44,59]. To understand the contributions of Néel and Brownian relaxation on the SLP, NPs can be placed in solvents more viscous than water such as glycerol that minimizes Brownian relaxation. Cobalt ferrite ($CoFe_2O_4$) NPs placed in increasing amounts of glycerol showed a sharp change in SAR from 420 to 90 W/g [60].

The SLP value is also proportional to the applied AC magnetic field strength and frequency. Maximum absorption of magnetic energy occurs when the characteristic fluctuation time is close to the period of the excitation field ($\omega\tau \approx 1$) [61,62]. This means that for a given f there is an optimum size that resonates well with the applied field. For a series of 17–47 nm-sized nano-octopods, maximum heat dissipation was observed for the smallest size at low AC fields (< 300–400 Oe) while the SLP increased linearly with size at higher fields (> 400 Oe) [49]. To better understand the size and field dependence of the heating efficiency in the nano-octopod system, AC magnetometry measurements were conducted at different applied field strengths. It has been demonstrated that at low fields, the magnetic hysteresis loop area is larger for smaller nano-octopods (17 nm), while at higher fields the hysteresis loop area is more enhanced for the bigger nano-octopods (47 nm). This effect was explained in terms of the relationship between the applied AC field (H_{AC}) and the calculated anisotropy field (H_A). When $H_{AC} < H_A$, the hysteresis loop area for the smaller nano-octopods were larger but with increasing H_{AC} the bigger NPs start to respond fully to the magnetic field excitation and hysteresis losses become more dominant. This in turn leads to a continuous increase in heating efficiency for the bigger sized nano-octopods while for the smaller nano-octopods the coercive field saturates much faster leading to lower heating efficiency at higher applied fields [42,49].

While it may sound counter intuitive, hysteresis losses are also possible for NPs that are superparamagnetic at room temperature due to the high frequencies used in magnetic hyperthermia measurements (i.e. hyperthermia AC frequencies used are typically larger than 100 kHz) [63]. At high frequencies, hysteresis occurs when the magnetization response of the NPs lag behind the applied field. Similar to a blocking temperature there is also a parameter called the blocking frequency, f_b, whereby at a frequency below f_b, the NPs are superparamagnetic but above this frequency, hysteresis is observed [64].

3.2. Chemical composition effects on the magnetic hyperthermia properties

Chemical tuning of the magnetic property of iron oxide-based NPs is critical in optimizing their performance in magnetic hyperthermia applications. Specifically, developing strongly magnetic nano-ferrites is important since the SLP value increases linearly with magnetization. Over the years, IONPs, of the Fe_3O_4 spinel ferrite phase, have been widely explored because of its low cost and biocompatibility. However, a limitation with this system is that the saturation magnetization of bulk magnetite is relatively low (92 emu/g) [49]. As such, other types of ferrites have been investigated including jacobsite ($MnFe_2O_4$), which has a higher magnetization (110 emu/g) in the bulk phase.

To better understand the effect of chemistry on the magnetic nature of iron oxide-based NPs, a first step is to look into the magnetic ordering in its crystal lattice. Magnetite and jacobsite belong to a special class of ferrites called spinels, which is represented by the general formula MFe_2O_4, where M can be any of the divalent metal ions. The spinel ferrite structure can be best described as a face-centered cubic arrangement of oxygen atoms, with M^{2+} and Fe^{3+} occupying any of two different crystallographic sites. These sites have tetrahedral or octahedral oxygen coordination, which are often termed A and B-sites, respectively [65,66]. In the unit cell, there are 8 A-sites and 16 B-sites, where the magnetic moments of the cations are aligned parallel with respect to one another. Between the A and B-sites, the magnetic ordering is anti-parallel and as there are twice as many B-sites than A-sites, there is a net moment of spins yielding ferrimagnetic ordering for the crystal. Fe_3O_4 has an inverse spinel structure with the tetrahedral A-sites occupied by Fe^{3+} ions while the octahedral B-sites are occupied by Fe^{2+} and Fe^{3+} ions. Therefore, Fe_3O_4 has an idealized magnetic moment of 4 μ_B per formula unit. On the other hand, $MnFe_2O_4$ has a mixed spinel structure with the A sites occupied by $Mn_{1-x}^{2+}Fe_x^{3+}(0 < x < 1)$ while the B sites are occupied by $Mn_x^{2+}Fe_{2-x}^{3+}$, which results in an idealized magnetic moment of 5 μ_B per formula

unit. The nature of the divalent metal cation and the magnetic ordering in the crystal lattice help explain the observed larger SLP for $MnFe_2O_4$ NPs (411 W/g) than that of similarly sized Fe_3O_4 NPs (333 W/g) [67].

Another way to tune the magnetism of spinel ferrites is to dope the system with non-magnetic Zn^{2+} ions resulting in a mixed ferrite phase such as $(Zn_xFe_{1-x})Fe_2O_4$. When$x \leq 0.4$, the Zn^{2+} ions occupying the tetrahedral A-sites can lower the antiferromagnetic coupling interactions between the Fe^{3+} ions in the A and B sites resulting in a net increase in magnetization for the Zn-doped system [68]. At higher Zn^{2+} doping levels, the antiferromagnetic coupling interactions between Fe^{3+} ions in each B-site become dominant and net magnetization decreases [68]. Spherical $(Zn_{0.4}Fe_{0.6})Fe_2O_4$ NPs were demonstrated to have higher magnetization and an SLP twice larger compared to its undoped Fe_3O_4 NP analog with values of 438.6 and 189.6 W/g, respectively [69]. These results showcase the importance of changing the chemical composition of magnetic materials to enhance magnetization that effectively leads to an increase in magnetic hyperthermia heating efficiency of magnetic NPs.

3.3. Shape anisotropy effects on the magnetic hyperthermia properties

The heating efficiency of a magnetic NP shows the dependence on the crystalline anisotropy and one route to tune the magnetic hyperthermia properties is to optimize the shape anisotropy by developing NPs with different morphologies. Along this line, cubic shaped IONPs have been synthesized because of their anticipated higher magnetization compared to their spherical counterparts. It has been demonstrated theoretically that cubic NPs have lower surface anisotropy compared to spheres due to smaller amount of disordered spins as a result of the flat surface of the cube and the fact that it is comprised mostly of low energy $<100>$ facets [70]. On the other hand, the curved surface of spherical NPs leads to a more pronounced surface spin canting (Fig. 4(a) and (b)) [70]. This phenomenon has been confirmed in experimental studies whereby the comparison of cubic and spherical IONPs, with similar magnetic volumes, showed about two-fold increase in SLP for the cubic analogs (356.2 vs. 189.6 W/g) [69]. The effect of shape on magnetic hyperthermia efficiency is further enhanced when the chemical composition is tuned as well in order to create intrinsically more magnetic NPs by doping IONPs with Zn^{2+} as previously discussed in Section 3.2. $Zn_{0.4}Fe_{2.6}O_4$ nanocubes showed an SLP value of 1019.2 W/g which is two times larger than that of $Zn_{0.4}Fe_{2.6}O_4$ nanospheres (438.6 W/g) (Fig. 4(c)) [69].

Khurshid et al. have demonstrated that optimization of shape anisotropy and not only saturation magnetization can be used to create materials with higher SLP [71]. Cubic shaped exchange coupled FeO/Fe_3O_4 NPs with higher shape and effective anisotropy but lower saturation magnetization compared to their spherical equivalents were reported to show a higher heating efficiency (200 vs 135 W/g) [71]. An important consequence of their result is that it provides a different approach to enhance the SLP by way of modulating the effective anisotropy and not simply increasing the saturation magnetization of a magnetic NP.

In addition, Fe_3O_4 nano-octopods (deformed cubes) were reported to show better heating efficiency compared to spheres due to enhanced shape anisotropy [49]. The deformed shape caused local symmetry breaking as a result of structural defects, broken symmetry bonds, and surface strain [49,72,73]. The nano-octopods were found to have an anisotropy (8×10^5 erg/cm^3 for 17 nm and 1.2×10^6 erg/cm^3 for 47 nm) that were an order of magnitude higher than that of bulk magnetite (1.1×10^5 erg/cm^3) and larger than that of cubic shaped magnetite NPs (7.7 and 4.2×10^5 erg/cm^3 for 20 and 40 nm sized nanocube, respectively) [74,75].

Iron oxide nanorods with tunable aspect ratio were also recently reported to show enhanced magnetic hyperthermia efficiency (862 W/g) compared to its cubic (314 W/g) and spherical (140 W/g) counterparts of similar magnetic volumes [76]. This effect was attributed to the larger saturation magnetization and effective anisotropy that originate from the pronounced unidirectional shape anisotropy of the nanorods [76].

NPs with different morphologies such as nanoflowers made of maghemite NPs have also been reported to show higher SLP values compared to dispersed NPs [77]. The increase in heating efficiency is attributed to the magneto-structural properties of the nanoflowers, which are composed of highly ordered nanocrystals that do not behave like isolated grains [77]. In addition, the nanoflowers exhibited lower anisotropy due to coalescence and crystal ordering of the individual grains while the spherical particles showed higher surface disorder and consequently, higher surface anisotropy. IONPs with novel and more complex shapes and structures such as hexagonal nanoplates, brick-like nanostructures, as well as nanoclusters of Mn-Zn-ferrite NPs have also demonstrated enhanced SLP [78–80]. These results showcase the importance of shape anisotropy in improving the magnetic hyperthermia performance of iron oxide-based NPs.

3.4. Effect of exchange coupling on the magnetic hyperthermia properties of spring nanomagnets

Exchange spring nanomagnets are composed of magnetically hard and soft phases, which can interact by magnetic exchange coupling to combine the best properties of each type of magnetic material [81–86]. The hard phase component provides a high coercive field while the soft phase component contributes toward a higher saturation magnetization for the coupled system (Fig. 5(a)). In these materials, the soft phase is pinned to the hard phase at the interface, which gives rise to characteristic features of having a reversible demagnetization curve while possessing a high energy product, $(BH)_{max}$, (Fig. 5(b))

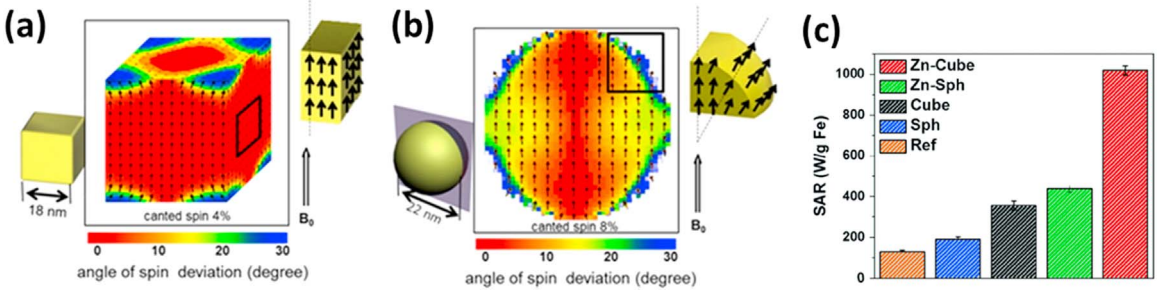

Fig. 4. Simulated magnetic spin states of (a) cubic and (b) spherical nanoparticles; the color map indicates the degree of spin canting in the presence of an external magnetic field (B_0), where red indicates non-deviated spins and blue indicates highly canted spin states; local spin states on the surfaces of nanoparticles are depicted on the right corners of (a) and (b). This illustration is reprinted with permission from reference [70], copyright (2012) American Chemical Society. (c) Comparison of the heating efficiency of spherical (Sph) and cubic (Cube) magnetite nanoparticles with Zn-doped magnetite spherical (Zn-Sph) and cubic (Zn-Cube) nanoparticles; the nanoparticle samples were compared against a commercial reference sample (Ref). This figure was reproduced from reference [69] with permission from the Royal Society of Chemistry.

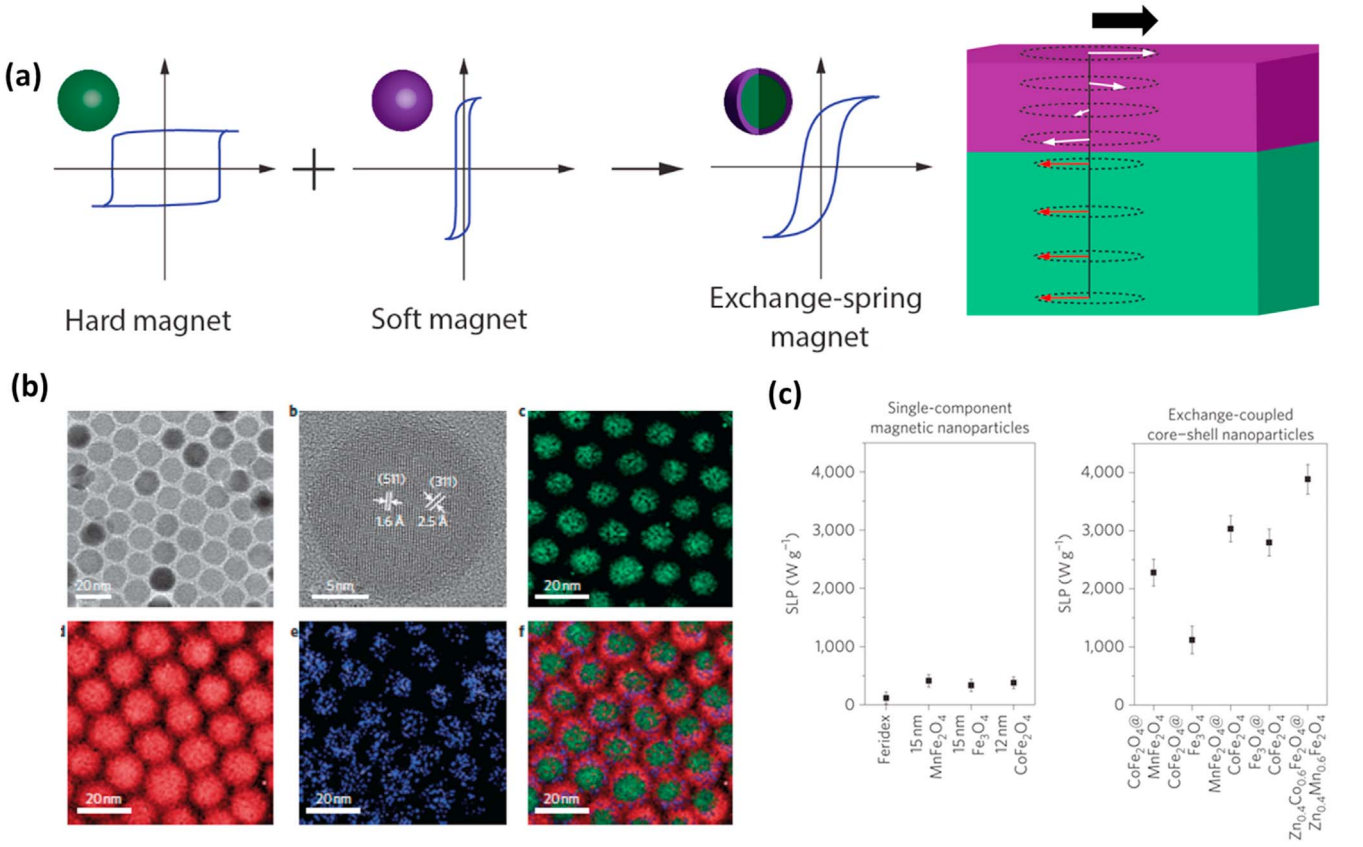

Fig. 5. (a) Illustration of the magnetic interactions in an exchange spring nanomagnet consisting of hard core and soft shell magnetic layers. (b) TEM image and electron energy loss spectroscopy (EELS) mapped-images of 15 nm $CoFe_2O_4$@$MnFe_2O_4$ exchange spring nanomagnet, and (c) plot showing the comparison of the heating efficiencies of single-component and core-shell nanoparticles. These figures were reprinted with permission from reference 67, copyright from the Macmillan Publishers Ltd: Nature Nanotechnology.

[70,81,85]. When an external magnetic field is applied, a twisted magnetic structure emerge as the magnetic moment of the soft phase reorient towards the direction of the external field, while remaining pinned at the interface of the hard magnetic phase(Fig. 5(a)) [85]. Removal of the magnetic field demagnetizes the soft phase and causes its magnetization to realign with the hard magnetic phase again; this phenomenon is referred to as the exchange spring process.

Over the past years, dramatically improved heating efficiency was observed for an exchange coupled nanomagnet made of 15 nm sized spherical $CoFe_2O_4$@$MnFe_2O_4$ (2280 W/g), compared to single component spherical NPs of 9 nm-sized $CoFe_2O_4$ (443 W/g), and 15 nm sized $MnFe_2O_4$ (411 W/g) [67]. Furthermore, the magnetism and anisotropy of exchange spring magnets can be tuned by combining different types of hard and soft magnetic spinel ferrites [67,81–84]; exchange coupled magnetic NPs composed of core@shell spherical structures of $CoFe_2O_4$@Fe_3O_4, Fe_3O_4@$CoFe_2O_4$, $CoFe_2O_4$@$MnFe_2O_4$, $MnFe_2O_4$@$CoFe_2O_4$, and $(Zn_{0.4}Co_{0.6})Fe_2O_4$@$(Zn_{0.4}Mn_{0.6})Fe_2O_4$ were synthesized and showed very high heating efficiencies between 1120 to 3886 W/g, which were an order of magnitude higher than single component Fe_3O_4, $MnFe_2O_4$, and $CoFe_2O_4$ (339–443 W/g) NPs (Fig. 5(c)) [67]. Extending the concept of exchange spring magnets with spherical morphology to other shapes, core-shell $Zn_{0.4}Fe2.6O_4$@$CoFe_2O_4$ cubic NPs with an average diameter of 60 nm were prepared and exhibited a coercivity 14 times larger than that of a pure $CoFe_2O_4$ nanocube analog. The high coercivity of the core-shell nanocube resulted in an ultra-high SLP value of 10600W/g [70]. The large coercivity due to the exchange anisotropy energy arising from interfacial interactions has a significant effect on the heating efficiency of ferrimagnetic NPs for magnetic hyperthermia applications. These results demonstrate that enhanced magnetic hyperthermia efficiency can be achieved by exploiting size, composition, and shape effects into creating exchange spring nanomagnets with tunable magnetic properties to achieve maximum SLP values.

3.5. Magnetic dipolar interactions: effect of nanochain and nanocluster formation on magnetic hyperthermia properties

In magnetic hyperthermia measurements, excitation of a single magnetic NP can only lead to a very small temperature increase of about 10^{-9} K [87], and NP concentrations on the order of 10^9 cm^{-3} is required to reach therapeutic temperatures [88]. At high concentrations, magnetic NPs can aggregate and form nano-assemblies, which can lead to changes in hyperthermia performance compared to well-dispersed magnetic NP formulations [89]. *In vivo*, uptake of magnetic NPs in sub-cellular vesicles such as lysosomes can lead to formation of magnetic NP aggregates that modify their magnetic hyperthermia properties due to dipolar interactions [90].

Magnetic dipolar interactions between neighboring NPs can be regulated by introducing capping ligands that increase inter-particle spacing [91,92]. The relationship between the energy associated with dipole-dipole interactions in relation to inter-particle spacing is described as follows [91]:

$$E_{d-d} = -(\mu_0 m_0^2)/(4\pi l^3) \quad (14)$$

where, m_0 is the NP magnetic moment and l is the particle-particle separation. Theoretical [93–103] and experimental studies [93,102,104–116] have been carried out in order to better understand the effects of magnetic dipolar interactions in hyperthermia measurements. Dipolar interaction effects on heating efficiency in magnetic hyperthermia have been shown to be either positive [75,77,93,104,115,117,118] or negative [94,96,113,119,120]. It has been demonstrated that the reduction or enhancement in the heating

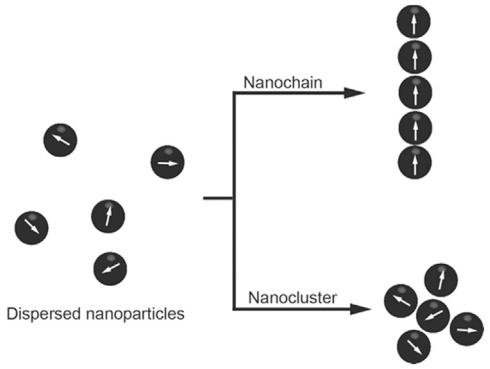

Fig. 6. Schematic representation of the different nano-assemblies that could form during AC magnetic field excitation.

efficiency of magnetic NPs is due to the formation of nano-assemblies during hyperthermia measurements. When exposed to an AC field, magnetic NPs can form linear aggregates of magnetically ordered structures such as chains (Fig. 6) [104]. Several groups have pointed out theoretically [93,102] and have shown experimentally [75,104,117,118,121] that chain-like structures can give rise to an increase in the heating efficiency of NPs. In order to maximize the heating efficiency it is necessary to assemble NPs into chains with a uniaxial anisotropy, which leads to hysteretic losses that can improve the heat power dissipation process [93,121]. This type of assembly leads to an enhancement of the effective anisotropy of the NPs due to the unidirectional magnetization orientation as a result of the dipolar coupling along the chain [121]. These particles that pack together in a chain-like formation display an increased ferromagnetic behavior with their moments locked in the direction of the magnetic field, which leads to an experimentally observed increase in heating efficiency [104,122,123]. Moreover, cubic NPs have been reported to self-assemble spontaneously into chains resulting in high surface magnetic anisotropy and consequently, very high hyperthermia efficiency [75]. Negative effects on heating efficiency by nanochain formation have likewise been reported but it was pointed out that while heating efficiency decreases with chain length there is an optimum chain length to achieve high SLP values [121,124]. Spontaneous formation of chains due to an increase in particle concentration may lead to coalescence and cluster formation, which reduces the heating efficiency of the magnetic NPs [75].

Modification of particle concentration has been employed to vary the strength of dipole-dipole interactions [120,125]. Salas et al. compared the heating efficiency of NPs (12 and 22 nm) dispersed in agar at two different concentrations (2.5 and 10 mg Fe/mL) and for both sizes, a reduction in the heat release at higher NP concentrations was observed due to aggregation resulting in formation of nanoclusters (based on hydrodynamic size measurement) and increased dipole-dipole interactions [126]. These NPs embedded in agar, were established to have randomly oriented anisotropy axis with regard to the direction of the external field or the particle magnetization vector based on magnetometry measurements. The angle (θ) between the easy axis and magnetization vector becomes finite for the NPs that were immobilized in agar and results in a reduction of the hysteresis area and heating efficiency [121]. Coral et al. also arrived at the same conclusion, wherein nanoclusters were shown to have lower heating efficiency with increasing cluster size and increasing number of particles in the cluster [120]. Moreover, the negative effects of nano-clustering to the heat dissipated during magnetic hyperthermia have been reported by other groups and an increase in the intensity of dipolar interactions resulted in a decrease in magnetic susceptibility and hysteresis losses leading to a reduction in the SLP value [96,119,125]. On the other hand, it has been reported in literature that favorable increase in heating effects were observed with clusters in the form of nanoflowers compared to individual particles [77]. These nanoflowers, however, contain single grains that have the same crystal orientation and all of its anisotropy axes are aligned giving it a different magnetic organization than the clusters discussed earlier in which the magnetic particles have randomly oriented anisotropy axes instead [77,120,125]. These studies have demonstrated that in most cases, magnetic dipolar interactions have favorable effects in magnetic hyperthermia heating when directionally oriented nanochains are formed but can lead to lower efficiencies when more disordered nanocluster assemblies arise during measurements.

4. Emerging research directions: magnetic imaging guided–hyperthermia

The ability to perform magnetic hyperthermia treatment in an imaging environment could revolutionize the way we diagnose and eradicate diseases. Combined hyperthermia and imaging could have several advantages including the ability to evaluate the local concentration of the magnetic NPs trapped inside diseased tissues, thereby enabling a more defined treatment plan to prevent overheating side effects. Moreover, the magnetic field used in hyperthermia could be provided by the same hardware utilized in magnetic imaging, which will facilitate the ease in adapting a coupled theranostic approach in disease management.

The development of a combined hyperthermia therapy with magnetic particle imaging (MPI) has been proposed [127–129]. MPI is an emerging imaging modality that is highly sensitive and directly detects magnetic NP tracers with no background signal coming from the tissue, thus, offering real-time, high resolution imaging of iron oxide-based NP tracers [130–132]. The magnetic NPs being developed for magnetic hyperthermia are also explored in MPI, whereby Néel and Brownian relaxation processes mainly dictate the heating mechanism in hyperthermia as well as the signal generation in MPI, making this coupled technology ideal in developing optimized magnetic NPs for theranostic applications.

Our group has recently reported and demonstrated for the first time the use of tailored iron oxide-based NPs for an MPI-guided magnetic hyperthermia (*h*MPI) approach [69]. In this study, shape and composition effects on MPI signal were investigated using magnetic particle spectroscopy by comparing spherical and cubic NPs of Fe_3O_4 and $Zn_{04}.Fe_{2.6}O_4$ with the same magnetic volume (3600–3700 nm^3). Magnetic hyperthermia experiments were also performed under static gradient fields similar to the one used in MPI (Fig. 7(a)–(c)). $Zn_{04}.Fe_{2.6}O_4$ spherical NPs showed a 2-fold enhancement in MPI signal compared to as-synthesized Fe_3O_4 and an 8-fold improvement compared to commercially available IONPs. Moreover, $Zn_{04}.Fe_{2.6}O_4$ cubic IONPs showed a 5-fold improvement in the heating efficiency compared to the commercially available sample with good MPI signal. Outside the field free region (FFR), the magnetization of the NPs is saturated and magnetic hyperthermia and MPI signal are non-existent. Thus, targeted and selective heating using magnetic hyperthermia can be achieved using MPI as a diagnostic tool (Fig. 7(d)).

5. Summary and outlook

Magnetic hyperthermia is a promising therapeutic approach, but in order to move this treatment modality to the clinical setting a better understanding of the behavior of magnetic NPs during hyperthermia measurements is required. As a first step, it is imperative to develop a standardized method of reporting hyperthermia efficiencies and to establish clinically acceptable AC magnetic field excitation conditions. Another key aspect that can enable the wide-spread adaption of magnetic hyperthermia to combat diseases is the development of optimized and well characterized magnetic NP hyperthermia agents. In this review we have presented how tuning of NP size, composition, shape, and exchange anisotropy can be utilized to improve the heating

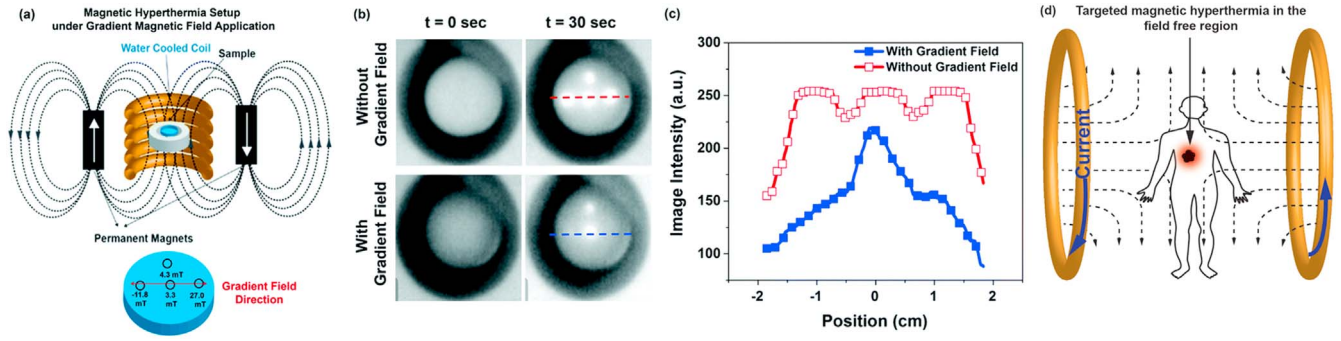

Fig. 7. (a) Schematic illustration of the magnetic hyperthermia measurement set-up under a gradient magnetic field similar to an MPI environment. (b) Thermal images of the nanocomposites with zinc-doped cubic iron oxide nanoparticles during magnetic hyperthermia measurement with and without gradient magnetic field application. (c) Thermal image intensity profiles of the center lines along the gradient field direction acquired 30 s after magnetic hyperthermia measurements with and without the application of a gradient magnetic field. All the hyperthermia measurements were performed at H=16 kA/m and f=380 kHz. Figures (a)–(c) were reproduced from reference 69 with permission from the Royal Society of Chemistry. (d) Schematic representation of an MPI-guided hyperthermia treatment whereby the signal is generated in the field free region (FFR). Outside the FFR, the magnetization of the magnetic nanoparticles is saturated and no signal is observed for both MPI and magnetic hyperthermia.

performance of iron oxide-based magnetic hyperthermia agents. Combining the advantageous effects of each parameter can result in the development of magnetic NPs with unprecedented heating efficiencies to enable effective *in vivo* applications. Moreover, due to the tendency of magnetic NPs to aggregate when internalized by the cells, a thorough study on how nano-assemblies affect the efficiency of the heat generation process is needed. Furthermore, emerging technologies that can provide novel diagnostic capabilities and facilitate targeted heating should be explored. Along this line, the combination of magnetic imaging technologies with magnetic hyperthermia, such as *h*MPI, is an exciting theranostic approach that could revolutionize the way we manage inoperable diseases in the clinic.

Acknowledgements

The authors acknowledge support from the Solid State and Materials Chemistry Program at NSF (DMR-1253358).

References

[1] N. Lee, D. Yoo, D. Ling, M.H. Cho, T. Hyeon, J. Cheon, Chem. Rev. 115 (2015) 10637–10689.
[2] G. Liu, J. Gao, H. Ai, X. Chen, Small 9 (2013) 1533–1545.
[3] L.H. Reddy, J.L. Arias, J. Nicolas, P. Couvreur, Chem. Rev. 112 (2012) 5818–5878.
[4] K.T. Nguyen, Y. Zhao, Acc. Chem. Res. 48 (2015) 3016–3025.
[5] H. Liang, X.B. Zhang, Y. Lv, L. Gong, R. Wang, X. Zhu, R. Yang, W. Tan, Acc. Chem. Res. 47 (2014) 1891–1901.
[6] M. Colombo, S. Carregal-Romero, M.F. Casula, L. Gutiérrez, M.P. Morales, I.B. Bohm, J.T. Heverhagen, D. Prosperi, W.J. Parak, Chem. Soc. Rev. 41 (2012) 4306–4334.
[7] T. Lammers, S. Aime, W.E. Hennink, G. Storm, F. Kiessling, Acc. Chem. Res. 44 (2011) 1029–1038.
[8] D. Yoo, J.H. Lee, T.H. Shin, J. Cheon, Theranostic magnetic nanoparticles, Acc. Chem. Res. 44 (2011) 863–874.
[9] J. Xie, G. Liu, H.S. Eden, H. Ai, X. Chen, Acc. Chem. Res. 44 (2011) 883–892.
[10] F.M. Kievit, M. Zhang, Acc. Chem. Res. 44 (2011) 853–862.
[11] D. Ho, X. Sun, S. Sun, Acc. Chem. Res. 44 (2011) 875–882.
[12] Y.W. Jun, J.W. Seo, J. Cheon, Acc. Chem. Res. 41 (2008) 179–189.
[13] M. Mahmoudi, S. Sant, B. Wang, S. Laurent, T. Sen, Adv. Drug Deliv. Rev. 63 (2011) 24–46.
[14] A. Hervault, N.T.K. Thanh, Nanoscale 6 (2014) 11553–11573.
[15] S. Laurent, D. Forge, M. Port, A. Roch, C. Robic, L. Vander Elst, R.N. Muller, Chem. Rev. 108 (2008) 2064–2110.
[16] K.M. Krishnan, IEEE Trans. Magn. 46 (2010) 2523–2558.
[17] A.G. Kolhatkar, A.C. Jamison, D. Litvinov, R.C. Willson, T.R. Lee, Int. J. Mol. Sci. 14 (2013) 15977–16009.
[18] E. Lim, T. Kim, S. Paik, S. Haam, Y. Huh, K. Lee, Chem. Rev. 115 (2015) 327–394.
[19] O. Veiseh, J.W. Gunn, M. Zhang, Adv. Drug Deliv. Rev. 62 (2010) 284–304.
[20] E.A. Périgo, G. Hemery, O. Sandre, D. Ortega, E. Garaio, F. Plazaola, F.J. Teran, Appl. Phys. Rev. 2 (2015) 041302.
[21] W. Wu, Z. Wu, T. Yu, C. Jiang, W.-S. Kim, Sci. Technol. Adv. Mater. 16 (2015) 023501.
[22] D. Ling, T. Hyeon, Small 9 (2013) 1450–1466.
[23] R. Hudson, RSC Adv. 6 (2016) 4262–4270.
[24] A.J. Giustini, A.A. Petryk, S.M. Casssim, J.A. Tate, I. Baker, P.J. Hoopes, Nano Life 01 (2010) 17–32.
[25] R.K. Gilchrist, R. Medal, W.D. Shorey, R.C. Hanselman, J.C. Parrott, C.B. Taylor, Ann. Surg. 146 (1957) 596–606.
[26] R.T. Gordon, J.R. Hines, D. Gordon, Med. Hypotheses 5 (1979) 83–102.
[27] A. Jordan, P. Wust, H. Fahling, W. John, A. Hinz, R. Feliz, Int. J. Hyperth. 9 (1993) 51–68.
[28] W.J. Atkinson, I.A. Brezovich, D.P. Chakraborty, IEEE Trans. Biomed. Eng. BME–31 (1984) 70–75.
[29] U. Gneveckow, A. Jordan, R. Scholz, V. Brüss, N. Waldöfner, J. Ricke, A. Feussner, B. Hildebrandt, B. Rau, P. Wust, Med. Phys. 31 (2004) 1444–1451.
[30] Magforce®: The nanomedicine company, (n.d.). ⟨http://www.magforce.de/en/unternehmen/ueber-uns.html⟩.
[31] F. Lu, A. Popa, S. Zhou, J.-J. Zhu, A.C.S. Samia, Chem. Commun. Camb. 49 (2013) 11436–11438.
[32] M. Pernia Leal, A. Torti, A. Riedinger, R. La Fleur, D. Petti, R. Cingolani, R. Bertacco, T. Pellegrino, ACS Nano 6 (2012) 10535–10545.
[33] S.D. Kong, W. Zhang, J.H. Lee, K. Brammer, R. Lal, M. Karin, S. Jin, Nano Lett. 10 (2010) 5088–5092.
[34] A. Riedinger, P. Guardia, A. Curcio, M.A. Garcia, R. Cingolani, L. Manna, T. Pellegrino, Nano Lett. 13 (2013) 2399–2406.
[35] H. Park, H.J. Park, J.A. Kim, S.H. Lee, J.H. Kim, J. Yoon, T.H. Park, J. Microbiol. Methods 84 (2011) 41–45.
[36] T.-K. Nguyen, H.T.T. Duong, R. Selvanayagam, C. Boyer, N. Barraud, Sci. Rep. 5 (2015) 18385.
[37] C. Yakacki, N. Satarkar, K. Gall, R. Likos, Z. Hilt, J. Appl. Polym. Sci. 112 (2009) 3166–3176.
[38] S.G. Kwon, T. Hyeon, Small 7 (2011) 2685–2702.
[39] K. Turcheniuk, A.V. Tarasevych, V.P. Kukhar, R. Boukherroub, S. Szunerits, Nanoscale 5 (2013) 10729–10752.
[40] A.H. Latham, M.E. Williams, C.O.N. Spectus, Acc. Chem. Res. 41 (2008) 411–420.
[41] C.L. Dennis, R. Ivkov, Int. J. Hyperth. 29 (2013) 715–729.
[42] H. Mamiya, J. Nanomater. 2013 (2013).
[43] M.A. Chuev, J. Hesse, J. Phys. Condens. Matter 19 (2007) 506201.
[44] R.E.. Rosensweig, J. Magn. Magn. Mater. 252 (2002) 370–374.
[45] M. Shliomis, Magn. Fluids, Sov. Phys. Uspekhi (Engl. Transl.). 17 (1974) 153–169.
[46] J. Carrey, B. Mehdaoui, M. Respaud, J. Appl. Phys. 109 (2011).
[47] B. Mehdaoui, A. Meffre, J. Carrey, S. Lachaize, L.M. Lacroix, M. Gougeon, B. Chaudret, M. Respaud, Adv. Funct. Mater. 21 (2011) 4573–4581.
[48] D.Ortega, Q.A.Pankhurst, Magnetic Hyperthermia, Nanoscience. Vol. 1 Nanostructures through Chemistry. P. O'brien (Ed.), 2013, Royal Society of Chemistry, Cambridge, UK.
[49] Z. Nemati, J. Alonso, L.M. Martinez, H. Khurshid, E. Garaio, J.A. Garcia, M.H. Phan, H. Srikanth, J. Phys. Chem. C. 120 (2016) 8370–8379.
[50] E. Natividad, M. Castro, A. Mediano, J. Magn. Magn. Mater. 321 (2009) 1497–1500.
[51] E. Natividad, M. Castro, A. Mediano, Appl. Phys. Lett. 92 (2008).
[52] I. Andreu, E. Natividad, Int. J. Hyperth. 29 (2013) 739–751.
[53] R.R. Wildeboer, P. Southern, Q.A. Pankhurst, J. Phys. D. Appl. Phys. 47 (2014) 495003.
[54] V. Connord, B. Mehdaoui, R. Tan, J. Carrey, M. Respaud, Rev. Sci. Instrum. 85 (2014) 093904.
[55] Y.-W. Jun, Y.-M. Huh, J.-S. Choi, J.-H. Lee, H.-T. Song, S. Kim, S. Yoon, K.-S. Kim, J.-S. Shin, J.-S. Suh, J. Cheon, J. Am. Chem. Soc. 127 (2005) 5732–5733.
[56] M.P. Morales, C.J. Serna, F. Bødker, S. Mørup, J. Phys. Condens. Matter 9 (1999) 5461–5467.
[57] M.P. Morales, S. Veintemillas-Verdaguer, M.I. Montero, C.J. Serna, A. Roig, L. Casas, B. Martínez, F. Sandiumenge, Chem. Mater. 11 (1999) 3058–3064.
[58] R. Chen, M.G. Christiansen, P. Anikeeva, ACS Nano 7 (2013) 8990–9000.
[59] E.C. Vreeland, J. Watt, G.B. Schober, B.G. Hance, M.J. Austin, A.D. Price, B.D. Fellows, T.C. Monson, N.S. Hudak, L. Maldonado-Camargo, A.C. Bohorquez,

C. Rinaldi, D.L. Huber, Chem. Mater. 27 (2015) 6059–6066.
[60] J.P. Fortin, C. Wilhelm, J. Servais, C. Ménager, J.C. Bacri, F. Gazeau, J. Am. Chem. Soc. 129 (2007) 2628–2635.
[61] M. Lévy, C. Wilhelm, J.-M. Siaugue, O. Horner, J.-C. Bacri, F. Gazeau, J. Phys. Condens. Matter 20 (2008) 204133.
[62] A.E. Deatsch, B.A. Evans, J. Magn. Magn. Mater. 354 (2014) 163–172.
[63] A. Giri, K. Chowdary, S.A. Majetich, Mater. Phys. Mech. 1 (2000) 1–10.
[64] D. Hasegawa, S. Naksaka, M. Sato, T. Ogawa, M. Takahashi, IEEE Trans. Magn. 42 (2006) 2805–2807.
[65] J.-H. Lee, Y.-M. Huh, Y. Jun, J. Seo, J. Jang, H.-T. Song, S. Kim, E.-J. Cho, H.-G. Yoon, J.-S. Suh, J. Cheon, Nat. Med. 13 (2007) 95–99.
[66] F. Fiorillo, I. Mayergoyz, Characterization and Measurement of Magnetic Materials, 1st ed., Academic Press, San Diego, CA, USA, 2004.
[67] J.-H. Lee, J.-T. Jang, J.-S. Choi, S.H. Moon, S.-H. Noh, J.-G.J.-W.J.-G.J.-W. Kim, J.-G.J.-W.J.-G.J.-W. Kim, I.-S. Kim, K.I. Park, J. Cheon, Nat. Nanotechnol. 6 (2011) 418–422.
[68] J.T. Jang, H. Nah, J.H. Lee, S.H. Moon, M.G. Kim, J. Cheon, Angew. Chem. Int. Ed. 48 (2009) 1234–1238.
[69] L.M. Bauer, S.F. Situ, M.A. Griswold, A.C.S. Samia, Nanoscale 8 (2016) 12162–12169.
[70] S.H. Noh, W. Na, J.T. Jang, J.H. Lee, E.J. Lee, S.H. Moon, Y. Lim, J.S. Shin, J. Cheon, Nano Lett. 12 (2012) 3716–3721.
[71] H. Khurshid, J. Alonso, Z. Nemati, M.H. Phan, P. Mukherjee, M.L. Fdez-Gubieda, J.M. Barandiaran, H. Srikanth, J. Appl. Phys. 117 (2015) 17A337.
[72] M. Jamet, W. Wernsdorfer, C. Thirion, V. Dupuis, P. Mélinon, A. Pérez, D. Mailly, Phys. Rev. B 69 (2004) 024401.
[73] L. Néel, J. Phys. Le. Radium 15 (1954) 225–239.
[74] B.D. Cullity, C.D. Graham, Introduction to Magnetic Materials, 2nd ed., Wiley-IEEE Press, Hoboken, NJ, USA, 2009.
[75] C. Martinez-Boubeta, K. Simeonidis, A. Makridis, M. Angelakeris, O. Iglesias, P. Guardia, A. Cabot, L. Yedra, S. Estradé, F. Peiró, Z. Saghi, P. Midgley, I. Conde-Leborán, D. Serantes, D. Baldomir, Sci. Rep. 3 (2013) 1652.
[76] R. Das, J. Alonso, Z. Nemati Porshokouh, V. Kalappattil, D. Torres, M.-H. Phan, E. Garaio, J.A. Garcia, J.L. Sánchez Llamazares, H. Srikanth, J. Phys. Chem. C 120 (2016) 10086–10093.
[77] P. Hugounenq, M. Levy, D. Alloyeau, L. Lartigue, E. Dubois, V. Cabuil, C. Ricolleau, S. Roux, C. Wilhelm, F. Gazeau, R. Bazzi, J. Phys. Chem. C 116 (2012) 15702–15712.
[78] J. Xie, C. Yan, Y. Zhang, N. Gu, Chem. Mater. 25 (2013) 3702–3709.
[79] H. Wang, T.B. Shrestha, M.T. Basel, M. Pyle, Y. Toledo, A. Konecny, P. Thapa, M. Ikenberry, K.L. Hohn, V. Chikan, D.L. Troyer, S.H. Bossmann, J. Mater. Chem. B 3 (2015) 4647–4653.
[80] M. Worden, M.A. Bruckman, M.-H. Kim, N.F. Steinmetz, J.M. Kikkawa, C. LaSpina, T. Hegmann, J. Mater. Chem. B 3 (2015) 6877–6884.
[81] E.F. Kneller, R. Hawig, IEEE Trans. Magn. 27 (1991) 3588–3600.
[82] F. Liu, Y. Hou, S. Gao, Chem. Soc. Rev. 43 (2014) 8098–8113.
[83] H. Zeng, J. Li, J.P. Liu, Z.L. Wang, S. Sun, Nature 420 (2002) 395–398.
[84] J.S. Jiang, J.E. Pearson, Z.Y. Liu, B. Kabius, S. Trasobares, D.J. Miller, S.D. Bader, D.R. Lee, D. Haskel, G. Srajer, J.P. Liu, J. Appl. Phys. 97 (2005) 10K311.
[85] E.E. Fullerton, J. Jiang, S. Bader, J. Magn. Magn. Mater. 200 (1999) 392–404.
[86] Q. Song, Z.J. Zhang, J. Am. Chem. Soc. 134 (2012) 10182–10190.
[87] Y. Rabin, Int. J. Hyperth. 18 (2002) 194–202.
[88] A.S. Eggeman, S.A. Majetich, D. Farrell, Q.A. Pankhurst, J. Appl. Phys. 43 (2007) 2451–2453.
[89] J.-P. Fortin, F. Gazeau, C. Wilhelm, Eur. Biophys. J. 37 (2008) 223–228.
[90] M. Lévy, F. Gazeau, J.-C. Bacri, C. Wilhelm, M. Devaud, Phys. Rev. B 84 (2011) 075480.
[91] C. Vestal, Q. Song, Z. Zhang, J. Phys. Chem. B 108 (2004) 18222–18227.
[92] G. Held, G. Grinstein, H. Doyle, S. Sun, C. Murray, Phys. Rev. B 64 (2001) 1–4.
[93] B. Mehdaoui, R.P. Tan, A. Meffre, J. Carrey, S. Lachaize, B. Chaudret, M. Respaud, Phys. Rev. B Condens. Matter Mater. Phys. 87 (2013) 1–10.
[94] C. Haase, U. Nowak, Phys. Rev. B 85 (2012) 045435.
[95] C. Verdes, B. Ruiz-Diaz, S.M. Thompson, R.W. Chantrell, A. Stancu, Phys. Rev. B 65 (2002) 174417.
[96] D. Serantes, D. Baldomir, C. Martinez-Boubeta, K. Simeonidis, M. Angelakeris, E. Natividad, M. Castro, A. Mediano, D.X. Chen, A. Sanchez, L.I. Balcells, B. Martinez, J. Appl. Phys. 108 (2010) 17–22.
[97] D. Kechrakos, K.N. Trohidou, Appl. Phys. Lett. 81 (2002) 4574.
[98] D. Kechrakos, K.N. Trohidou, Phys. Rev. B 58 (1998) 12169–12177.
[99] J. Dormann, D. Fiorani, E. Tronc, J. Magn. Magn. Mater. 202 (1999) 251–267.
[100] J.-O. Andersson, C. Djurberg, T. Jonsson, P. Svedlindh, P. Nordblad, Phys. Rev. B 56 (1997) 13983–13988.
[101] G.T. Landi, Phys. Rev. B Condens. Matter Mater. Phys. 89 (2014) 014403.
[102] R. Fu, Y.Y. Yan, C. Roberts, AIP Adv. 5 (2015) 127232.
[103] I. Conde-Leboran, D. Baldomir, C. Martinez-Boubeta, O. Chubykalo-Fesenko, M. del Puerto Morales, G. Salas, D. Cabrera, J. Camarero, F.J. Teran, D. Serantes, J. Phys. Chem. C 119 (2015) 15698–15706.
[104] S.L. Saville, B. Qi, J. Baker, R. Stone, R.E. Camley, K.L. Livesey, L. Ye, T.M. Crawford, O. Thompson Mefford, J. Colloid Interface Sci. 424 (2014) 141–151.
[105] J.L. Dormann, F. D'Orazio, F. Lucari, E. Tronc, P. Prené, J.P. Jolivet, D. Fiorani, R. Cherkaoui, M. Noguès, Phys. Rev. B 53 (1996) 14291–14297.
[106] T. Jonsson, J. Mattsson, C. Djurberg, F.A. Khan, P. Nordblad, P. Svedlindh, Phys. Rev. Lett. 75 (1995) 4138–4141.
[107] T. Jonsson, J. Mattsson, P. Nordblad, P. Svedlindh, J. Magn. Magn. Mater. 168 (1997) 269–277.
[108] S.H. Masunaga, R.F. Jardim, R.S. Freitas, J. Rivas, Appl. Phys. Lett. 98 (2011).
[109] S.H. Masunaga, R.F. Jardim, P.F.P. Fichtner, J. Rivas, Phys. Rev. B 80 (2009) 184428.
[110] S.H. Masunaga, R.F. Jardim, J. Rivas, J. Appl. Phys. 109 (2011) 07B521.
[111] J. Sung Lee, R.P. Tan, J. Hua, Wu, Y. Keun Kim, Appl. Phys. Lett. 99 (2011) 062506.
[112] C.L. Dennis, A.J. Jackson, J.A. Borchers, R. Ivkov, A.R. Foreman, J.W. Lau, E. Goernitz, C. Gruettner, J. Appl. Phys. 103 (2008) 19–22.
[113] A. Urtizberea, E. Natividad, A. Arizaga, M. Castro, A. Mediano, J. Phys. Chem. C 114 (2010) 4916–4922.
[114] C. Martinez-Boubeta, K. Simeonidis, D. Serantes, I. Conde-Leborán, I. Kazakis, G. Stefanou, L. Peña, R. Galceran, L. Balcells, C. Monty, D. Baldomir, M. Mitrakas, M. Angelakeris, Adv. Funct. Mater. 22 (2012) 3737–3744.
[115] P. de la Presa, Y. Luengo, V. Velasco, M.P. Morales, M. Iglesias, S. Veintemillas-Verdaguer, P. Crespo, A. Hernando, J. Phys. Chem. C 119 (2015) 11022–11030.
[116] J.M. Orozco-Henao, D.F. Coral, D. Muraca, O. Moscoso-Londoño, P. Mendoza Zélis, M.B. Fernandez van Raap, S.K. Sharma, K.R. Pirota, M. Knobel, J. Phys. Chem. C 120 (2016) 12796–12809.
[117] E. Alphandéry, I. Chebbi, F. Guyot, M. Durand-Dubief, Int. J. Hyperth. 29 (2013) 801–809.
[118] E. Alphandéry, S. Faure, O. Seksek, F. Guyot, I. Chebbi, ACS Nano 5 (2011) 6279–6296.
[119] M.E. Materia, P. Guardia, A. Sathya, M. Pernia Leal, R. Marotta, R. Di Corato, T. Pellegrino, Langmuir 31 (2015) 808–816.
[120] D.F. Coral, P.M. Zélis, M. Marciello, M. Del Puerto, A. Craievich, F.H. Sanchez, M.B.F. Van Raap, Langmuir 32 (2016) 1201–1213.
[121] D. Serantes, K. Simeonidis, M. Angelakeris, O. Chubykalo-Fesenko, M. Marciello, M. Del Puerto Morales, D. Baldomir, C. Martinez-Boubeta, J. Phys. Chem. C 118 (2014) 5927–5934.
[122] D. Serantes, D. Baldomir, M. Pereiro, B. Hernando, V.M. Prida, J.L. Sánchez Llamazares, a Zhukov, M. Ilyn, J. González, J. Phys. D. Appl. Phys. 42 (2009) 215003.
[123] M. Varón, M. Beleggia, T. Kasama, R.J. Harrison, R.E. Dunin-Borkowski, V.F. Puntes, C. Frandsen, Sci. Rep. 3 (2013) 1234.
[124] L.C. Branquinho, M.S. Carrião, A.S. Costa, N. Zufelato, M.H. Sousa, R. Miotto, R. Ivkov, A.F. Bakuzis, Sci. Rep. 3 (2013) 2887.
[125] J.G. Ovejero, D. Cabrera, J. Carrey, T. Valdivielso, G. Salas, F.J. Teran, Phys. Chem. Chem. Phys. 18 (2016) 10954–10963.
[126] G. Salas, J. Camarero, D. Cabrera, H. Takacs, M. Varela, R. Ludwig, H. Dähring, I. Hilger, R. Miranda, M.D.P. Morales, F.J. Teran, J. Phys. Chem. C 118 (2014) 19985–19994.
[127] K. Murase, H. Takata, Y. Takeuchi, S. Saito, Phys. Med. 29 (2013) 624–630.
[128] K. Murase, M. Aoki, N. Banura, K. Nishimoto, A. Mimura, T. Kuboyabu, I. Yabata, Open J. Med. Imaging 05 (2015) 85–99.
[129] T. Kuboyabu, I. Yabata, M. Aoki, N. Banura, K. Nishimoto, A. Mimura, K. Murase, Open J. Med. Imaging 06 (2016) 1–15.
[130] B. Gleich, J. Weizenecker, Nature 435 (2005) 1214–1217.
[131] M.H. Pablico-Lansigan, S.F. Situ, A.C.S. Samia, Nanoscale 5 (2013) 4040–4055.
[132] L.M. Bauer, S.F. Situ, M.A. Griswold, A.C.S. Samia, J. Phys. Chem. Lett. 6 (2015) 2509–2517.